Supporting information

Synthesis of ultrathin wrinkle-free PdCu alloy nanosheets for *d*-band electrons modulating efficient methanol oxidation

Jinchang Fan, Shansheng Yu, Kun Qi, Chang Liu, Lei Zhang, Haiyan Zhang, Xiaoqiang Cui and Weitao Zheng**

State Key Laboratory of Automotive Simulation and Control, Department of Materials Science, Jilin University, Changchun 130012, People's Republic of China

Corresponding Author: E-mail: xqcui@jlu.edu.cn (XQ Cui), wtzheng@jlu.edu.cn (WT Zheng)

Chemicals and Materials. Palladium acetylacetonate ($Pd(acac)_2$, 99 %), palladium black (99.95%) and platinum black (99.97%) were obtained from Sigma Aldrich (USA). Copper acetylacetonate ($Cu(acac)_2$, 97 %) were obtained from Aladdin reagent (China). Cetyltrimethyl ammonium bromide (CTAB, AR), polyvinylpyrrolidone (PVP MW=40000, AR), N,N-dimethylformamide (DMF, AR), n-butylamine ($C_4H_{11}N$, AR), potassium hydroxide (KOH, AR), methanol (CH_3OH, AR) and sulphuric acid (H_2SO_4, AR) were all purchased from Sinopharm Chemical Reagent (China). Carbon monoxide (ultra-purity) was purchased from Xin'guang gas Co., (Changchun, China). Nafion-ethanol solution was obtained from Adamas-beta Chemical Co., (Switzerland). Milli-Q deionized water (DI water, 18.2 MΩ cm^{-1}) was used in all experiments. All reagents were used as received without further purification.

Characterization. Transmission electron microscopy (TEM) and high-resolution transmission electron microscopy (HRTEM) were acquired by using a JEM-2100F transmission electron microscope (JEOL Co., Japan). High-angle annular dark field scanning TEM (HAADF-STEM) and energy-dispersive X-ray spectroscopy (EDX) mapping were performed on a Tecnai F30 microscope operated at 300 kV. Atomic force microscope (AFM) images were obtained by deposition of sample on a Si wafer and investigated by using ScanAsyst in air with tapping mode (Dimension Icon, Veeco Instruments/Bruker, Germany). X-ray photoelectron spectroscopy (XPS) data was acquired with an ESCALAB-250 instrument (Thermo Fisher Scientific, USA), performed with a monochromatic Al-Kα (1486.6 eV) radiation source and a hemisphere detector with an energy resolution of 0.1 eV. Inductively coupled plasma mass spectrometry (ICP-MS) data was collected with an ELAN 9000/DRC ICP-MS system. X-ray diffraction (XRD) patterns were obtained using a Bragg–Brentano diffractometer (D8-tools, Germany).

Synthesis of PdCu alloy nanosheets. In a typical synthesis of Pd_4Cu_1 alloy NSs, 30 mg of $Pd(acac)_2$, 5.2 mg of $Cu(acac)_2$, 50 mg of PVP and 100mg of CTAB were added into a mixed solution, containing 10 mL of DMF, 2 mL of water and 500 μL of n-butylamine. The solution was under vigorous stirring for 30 min to form a homogeneous solution and then transferred into a 25 mL Teflon-lined autoclave. After being bubbled with CO for 10 min, the vessel was sealed and heated from room temperature to 150 °C in 30 min and kept at this temperature for another 3 h before it was naturally cooled to room temperature. The resulting products were collected by centrifugation (11000 rpm, 10 min) and washed with cyclohexane and ethanol (1:4) three times. The synthetic conditions for $Pd_{0.8}Cu_1$, $Pd_{2.5}Cu_1$ and $Pd_{6.5}Cu_1$ alloy nanocrystals were similar to that of Pd_4Cu_1 alloy NSs, except of changing the amounts of $Cu(acac)_2$ to 26 mg, 8.7 mg and 3.7 mg, respectively.

Electrochemical measurements. The electrochemical measurements were conducted on a CHI650D electrochemical workstation. A L-type glassy carbon electrode (diameter: 5 mm, area: 0.196 cm^2), a Ag/AgCl electrode, and a platinum foil (1 cm × 1 cm) were used as the working, reference, and counter electrodes, respectively. For preparation of the working electrode (WE), 24 μL of an ethanol suspension of the catalysts were dispersed on WE, then 6 μL of Nafion-ethanol solution (0.05 % wt.) was covered. The loading amounts of Pd-based catalysts were kept constant in terms of Pd as 10μg/cm^2 based on the ICP-MS measurement. Before data collection, all working electrodes were cleaned by steady-state potential sweeping from −0.9 to 0.5 V at 50 mV s^{-1} in N_2-saturated 1 M KOH solution for 40 cycles.

The ECSA of the catalyst was calculated from the area in the reduction peak of the palladium oxide using the following equation: ECSA = Q / (m**q)*, where Q is the

surface charge for oxygen desorption, m is the metal loading and q is the charge of desorbing a monolayer of oxygen on the Pd surface (424 μC cm^{-2}), and the scan range was chosen from -0.9 V to 0.2 V to avoid the formation of multilayered oxygen on the Pd surface. The MOR catalytic activity and cycling stability measurements were carried out by CV scanning form -0.8 V to 0.3 V with a scan rate of 50 mV s^{-1} in N_2-saturated 1 M KOH + 1 M CH_3OH solution. The long-term stability test was obtained at a constant potential of -0.22 V by chronoamperometric scanning.

In the CO stripping test, the catalysts were saturated with CO by bubbling CO gas in 0.5 M H_2SO_4 while holding the working electrode at -0.1 V for 8 min. Then non-adsorbed CO was removed by bubbling N_2 for 10 min. CO striping CV was performed between -0.1 - 1.3 V with a scan rate of 50 mV/s.

DFT calculations. All theoretical calculations were conducted using spin-polarized density functional theory by CASTEP code. The exchange-correlation energies were calculated using the generalized gradient approximation as parameterized by Perdew-Burke-Ernzerhof. The ultrasoft pseudopotentials were considered to describe the coupling between ionic core and valence electrons. LDA+U formalism was applied, in which a Hubbard U value was 2.0/2.5 eV for Pd/Cu atom for the valence *d* shell. The Monkhorst-Pack mesh *k*-point (3×3×1) was used for the slab calculations. The cutoff energy for the plane-wave basis set was set to be 400 eV. A convergence accuracy of 1.0×10^{-6} eV per atom was set for the self-consistent field calculation. A vacuum region of 13 Å was used, resulting in negligible interaction between the periodic slabs along the z direction.

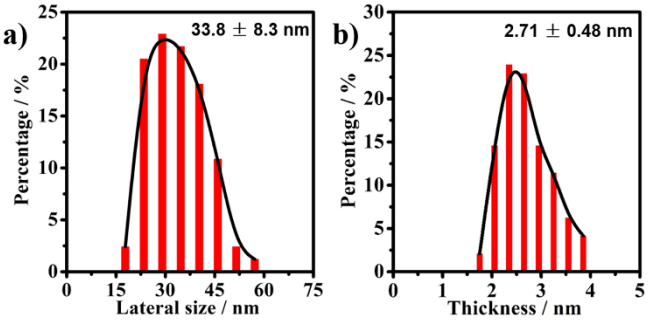

Fig. S1 Histogram of (a) lateral size and (b) thickness distribution of Pd_4Cu_1 NSs.

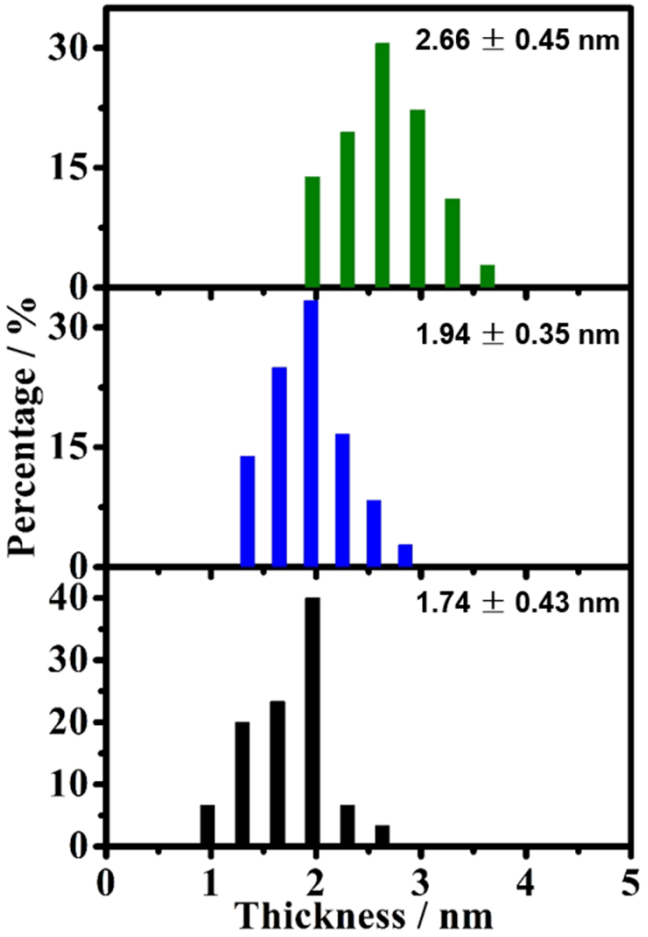

Fig. S2 Histogram of thickness distribution of Pd_4Cu_1 NSs obtained at the different reaction time.

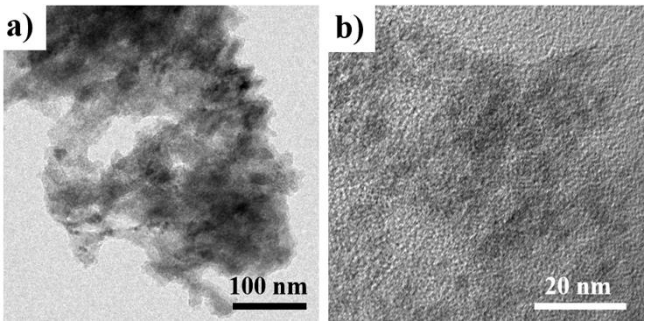

Fig. S3 (a) TEM and (b) HRTEM images of the products only with the Cu precursor.

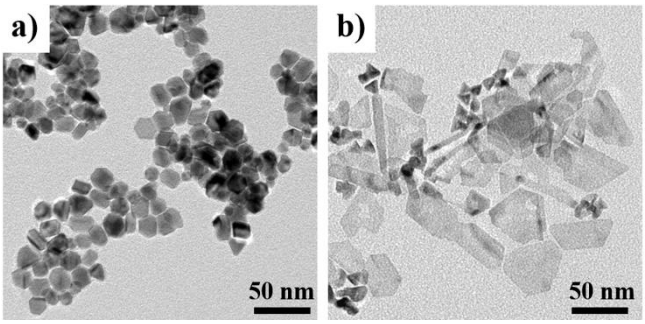

Fig. S4 TEM images of the products prepared only with the Pd precursor: (a) without n-butylamine and (b) with n-butylamine.

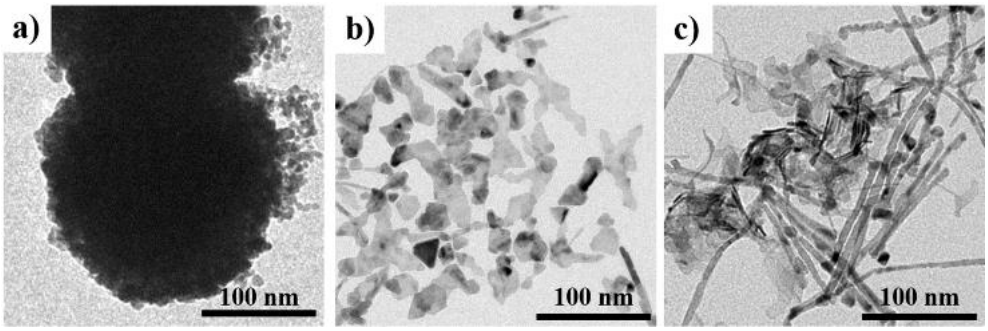

Fig. S5 Representative TEM images of the products collected from the reaction with the same conditions of Pd_4Cu_1 NSs but in the absence of (a) PVP, (b) CTAB, and (c) H_2O.

Fig. S5a shows that PVP serves as an effective coating agent to stabilize the products against agglomeration. While nanodendritic and nanorod morphology appeared in the absence of CTAB and H_2O, respectively (Fig. S5b and S5c). The results suggest that CTAB and H_2O served as a structure-directing agent to force the formation of hexagonal or trapezoid sheets morphology.

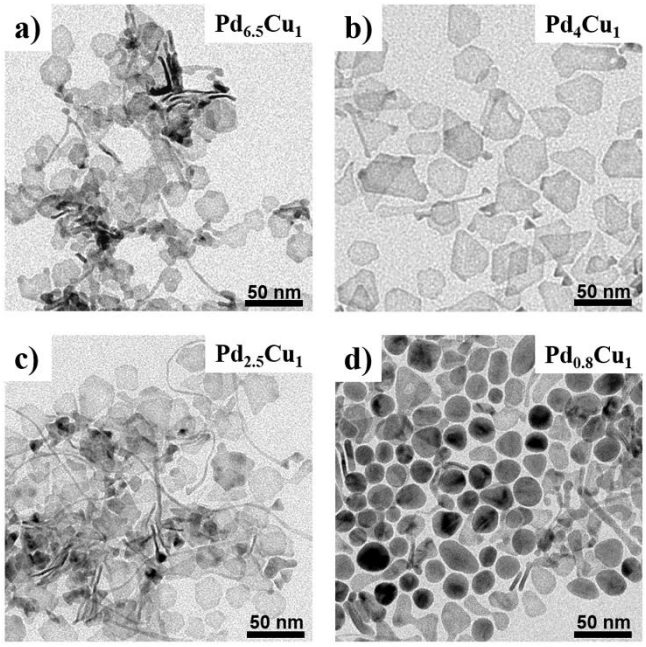

Fig. S6 (a-d) TEM images of PdCu nanostructures with different Pd/Cu ratio.

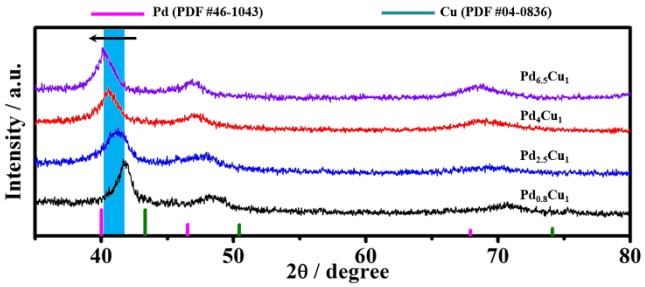

Fig. S7 XRD image of PdCu nanostructures with different Pd/Cu ratio.

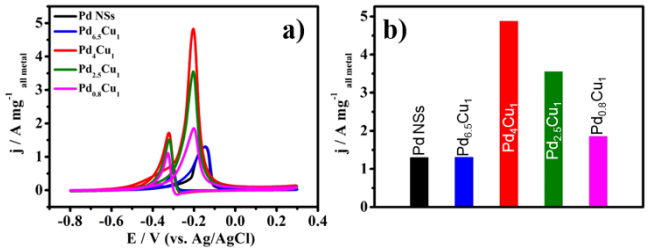

Fig. S8 (a) Cyclic voltammograms curves and (b) histogram of MOR mass activities of Pd NSs and PdCu nanostructures with different Pd/Cu ratio in 1 M KOH + 1 M CH_3OH.

The electrocatalytic performance of PdCu nanostructures depends on the Pd/Cu ratio, and the Pd_4Cu_1 NSs exhibited the best MOR activity.

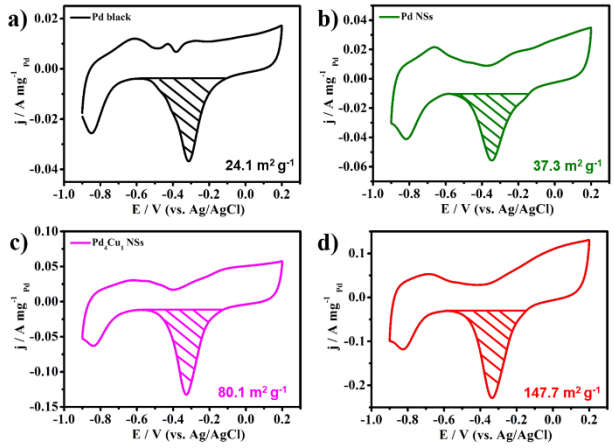

Fig. S9 The calculated ECSA of (a) Pd black, (b) Pd NSs, (c) Pd_4Cu_1 NPs and (d) Pd_4Cu_1 NSs.

The ECSA of benchmark Pd black in our work was calculated as of 24.1 m^2 g^{-1}, which is in consist with the results of the reported works, 23.3 m^2 g^{-1} (*Small*, 2017, 13, 1602970); 23.8 m^2 g^{-1} (*Small*, 2016, 12, 706-712); 24.2 m^2 g^{-1} (*J. Mater. Chem. A*, 2014, 2, 18177-18183).

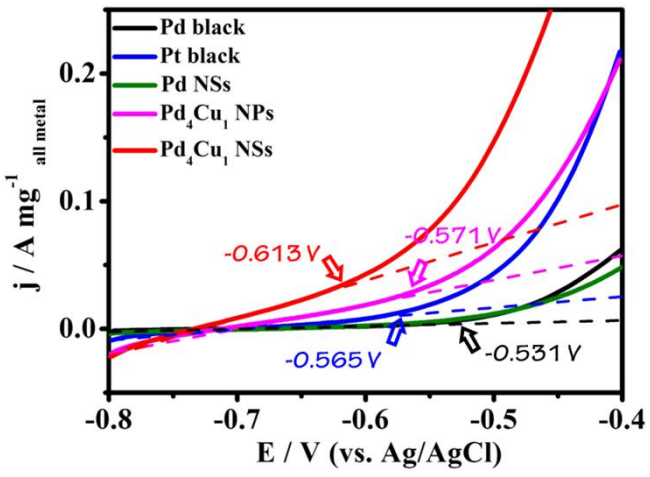

Fig. S10 Amplified area of positive scanning in Figure 5a to distinguish the onset-potential of five kinds of catalysts.

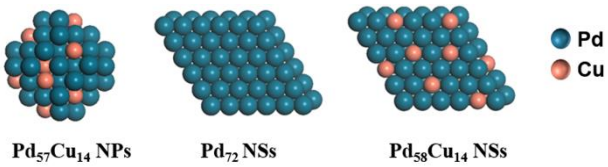

Fig. S11 The theoretical models of $Pd_{57}Cu_{14}$ NPs, Pd_{72} NSs and $Pd_{58}Cu_{14}$ NSs.

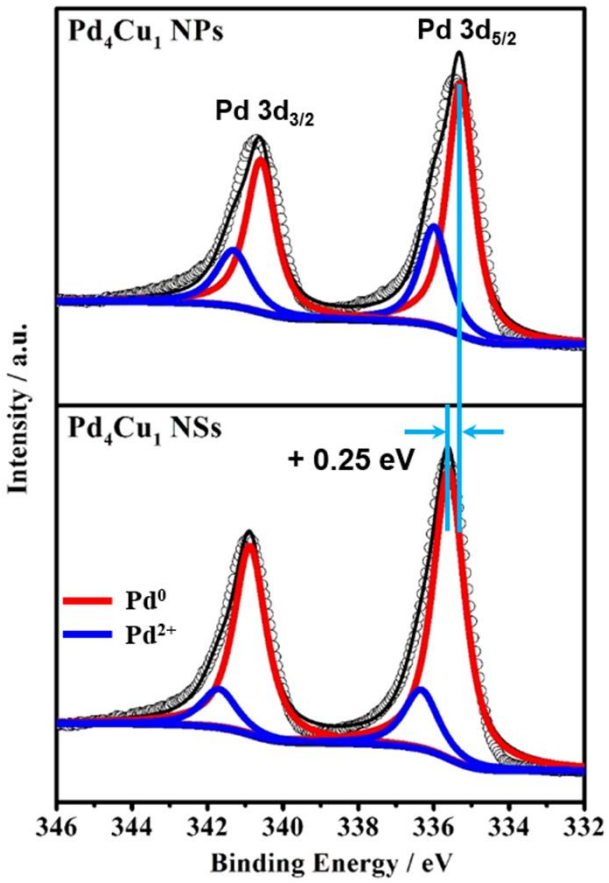

Fig. S12 The Pd 3d XPS spectra of Pd_4Cu_1 NPs and Pd_4Cu_1 NSs.

The core-level XPS peak of Pd in Pd_4Cu_1 NSs shifted about 0.25 eV towards higher energy than that of Pd_4Cu_1 NPs, indicating a down-shift of *d*-band of Pd_4Cu_1 NSs.

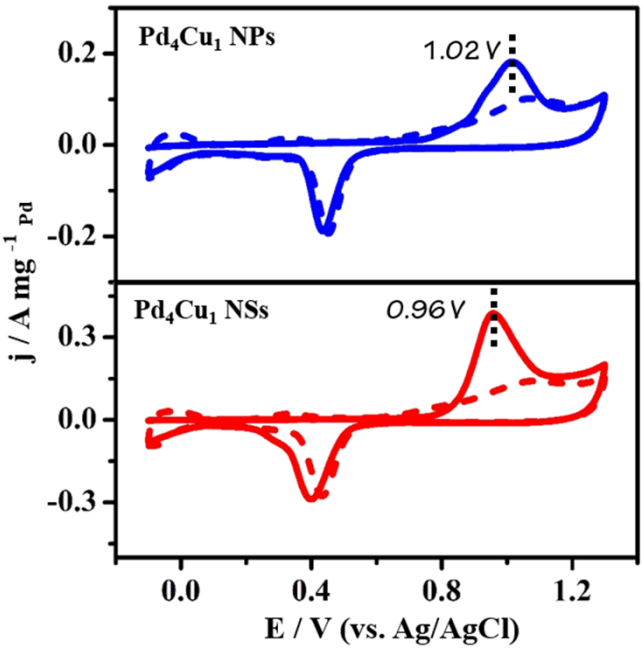

Fig. S13 CO stripping voltammetry of the Pd_4Cu_1 NPs and Pd_4Cu_1 NSs in 0.5 M H_2SO_4. The solid line is from the first scanning cycle and the dashed line is from the second scanning cycle.

We also calculated the ECSA from the CO stripping voltammetry by assuming the oxidation of a monolayer of CO on Pd corresponds to a charge of 420 μC cm^{-2}. The ECSA of Pd_4Cu_1 NSs was calculated to be of 180.3 m^2 g^{-1}, which is higher than the value of 147.7 m^2 g^{-1} obtained from CV curves in 1M KOH in Fig. S9d.

Calculations of the specific surface area for a Pd_4Cu_1 NSs by a geometry model:

We established a nanosheet geometry model with the lateral size of 33.8 nm (an edge length of 16.9 nm) and a thickness of 2.71 nm for calculating the specific surface area (Fig. S14). The surface area was calculated as $S = \frac{\sqrt{3}}{2} \times 16.9 \times 16.9 \times \frac{1}{2} \times 6 \times 2 + 6 \times 16.9 \times 2.71 = 1758.87$ nm^2. The volume was calculated as $V = \frac{\sqrt{3}}{2} \times 16.9 \times 16.9 \times \frac{1}{2} \times 6 \times 2.71 = 2010.92$ nm^3. The density was calculated as $\rho = \frac{4}{5} \times 12.023(\rho\ \mathrm{Pd}) + \frac{1}{5} \times 8.9(\rho\ \mathrm{Cu}) = 11.40$ g cm^{-3}. Thus, the specific surface area was calculated as $B = S / (V^* \rho) = 76.72$ m^2 g^{-1}, which is smaller than the ECSA value of 147.7 m^2 g^{-1} calculated by the electrochemistry measurement. This difference is probably due to the synergistic effect between Pd and Cu, abundant of high-active sites of atomic steps and unsaturated atoms on the surface of PdCu nanosheets.

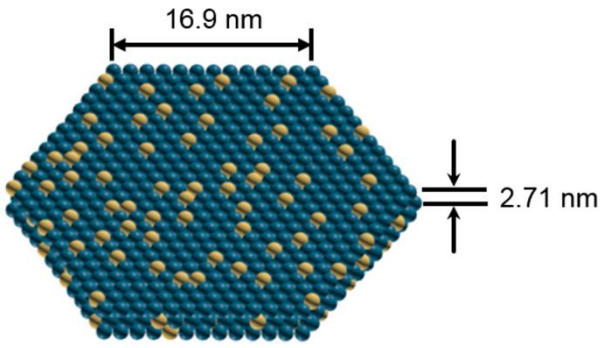

Fig. S14 Schematically illustrating a model for Pd_4Cu_1 NSs.

Table S1. Summary of MOR properties of the high-performance electrode materials reported in recent literatures.

Catalyst	**Morphology**	**Mass activity (A/mg $_{Pd\ or\ Pt}$)**	**Reference**
Pd_4Cu_1	nanosheets	5.6	This work
Pt/Ni(OH)$_2$/rGO	nanoparticles	1.07	Nat. Comm. 2015, 6, 10035
v-PdCuCo	anisotropic	0.17	Adv. Mater. 2017, 1704171
PtCu	five-fold-twinned nanoframes	2.26[a]	Adv. Mater. 2016, 28, 8712–8717
Au/Ag/Pt	nanoparticles	1	Adv. Mater. 2015, 27, 5573-5577
PdAg/$Ti_{0.5}Cr_{0.5}N$	nanoparticles	0.844	ACS Nano 2014 8 (6), 6106-6113
Pt/Ag	hollow popcorns	1.64	ACS Nano 2012 6 (8), 7397-7405
Pd_{45} Pt_{55}	nanowires	1.97	Adv. Mater. 2012, 24, 2326-2331
$Cu_4Pt_2Pd_2$	nanoparticles	4.29	ACS Appl. Mater. Interfaces 2017, 9, 25995−26000
Pd_1Cu_5	nanocages	1.09	J. Mater. Chem. A, 2018, 6, 3906-3912
Pd_7Cu_3/rGO	nanofinger	2.025	Electrochim. Acta 2018, 260, 47-54
PdCu/VrGO	nanoparticles	0.76	J. Power Sources 2015, 278, 725-732

General reaction conditions are 1M KOH + 1M methanol.
[a]The reaction solution is 0.5M KOH + 1M methanol.